Title

MRI perfusion measurements calculated using advanced deconvolution techniques predict survival in recurrent glioblastoma treated with bevacizumab

Journal

Journal of Neuro-Oncology, 122(3)

ISSN

0167-594X

Authors

Harris, RJ
Cloughesy, TF
Hardy, AJ
et al.

Publication Date

2015-05-22

DOI

10.1007/s11060-015-1755-8

Peer reviewed

J Neurooncol (2015) 122:497–505
DOI 10.1007/s11060-015-1755-8

CLINICAL STUDY

MRI perfusion measurements calculated using advanced deconvolution techniques predict survival in recurrent glioblastoma treated with bevacizumab

Robert J. Harris[1,2] · Timothy F. Cloughesy[3] · Anthony J. Hardy[1,2] · Linda M. Liau[4] · Whitney B. Pope[1] · Phioanh L. Nghiemphu[3] · Albert Lai[3] · Benjamin M. Ellingson[1,2,5]

Received: 19 November 2014 / Accepted: 8 March 2015 / Published online: 15 March 2015

Abstract Bevacizumab is a therapeutic drug used in treatment of recurrent glioblastoma to inhibit angiogenesis. Treatment response is often monitored through the use of perfusion MRI measures of cerebral blood volume, flow, and other pharmacokinetic parameters; however, most methods for deriving these perfusion parameters can produce errors depending on bolus kinetics. Recently, a number of new methods have been developed to overcome these challenges. In the current study we examine cerebral blood volume and blood flow characteristics in 45 recurrent glioblastoma patients before and after treatment with bevacizumab. Perfusion MRI data was processed using a standard single value decomposition (SVD) technique, two block-circulant SVD techniques, and a Bayesian estimation technique. A proportional hazards model showed that patients with a large decrease in relative blood volume (RBV) after treatment had extended overall survival ($P = 0.0048$). Patients with large pre-treatment relative blood flow (RBF) showed extended progression-free survival ($P = 0.0216$) and overall survival ($P = 0.0112$), and patients with a large decrease in RBF following treatment showed extended overall survival ($P = 0.0049$). These results provide evidence that blood volume and blood flow measurements can be used as biomarkers in patients treated with bevacizumab.

Keywords DSC-MRI · CBV · CBF · MTT · Deconvolution · Glioblastoma

✉ Benjamin M. Ellingson
bellingson@mednet.ucla.edu

[1] UCLA Brain Tumor Imaging Laboratory (BTIL), Department of Radiological Sciences, David Geffen School of Medicine, University of California Los Angeles, 924 Westwood Blvd., Suite 615, Los Angeles, CA 90024, USA

[2] Department of Biomedical Physics, David Geffen School of Medicine, University of California Los Angeles, Los Angeles, CA, USA

[3] Department of Neurology, David Geffen School of Medicine, University of California Los Angeles, Los Angeles, CA, USA

[4] Department of Neurosurgery, David Geffen School of Medicine, University of California Los Angeles, Los Angeles, CA, USA

[5] Department of Bioengineering, Henry Samueli School of Engineering and Applied Science, University of California Los Angeles, Los Angeles, CA, USA

Introduction

Glioblastoma multiforme (GBM) is the most common and aggressive type of primary brain tumor, with approximately 10,000 new cases diagnosed in the United States every year. [1] Despite aggressive treatment including surgical resection and concomitant radiation and chemotherapy, median survival is only approximately 12–15 months [2–4]. GBM and other malignant gliomas flourish and accelerate their growth rates by both co-opting existing vasculature and inducing neovascularization [5–7]. Thus, a new class of therapeutics called anti-angiogenic agents has been developed to combat the formation of these new blood vessels. Bevacizumab, a humanized monoclonal antibody to VEGF, is currently the only anti-angiogenic agent FDA-approved for use in recurrent GBM. As treatment with anti-angiogenic agents is expected to have a significant and direct impact on tumor vasculature, there is growing interest in surrogate biomarkers for evaluating changes in blood volume and blood flow using perfusion MRI.

Dynamic susceptibility contrast (DSC)-MRI is a specific perfusion MR technique that is often used to estimate

cerebral blood volume (CBV), cerebral blood flow (CBF), and mean transit times (MTT) in patients with brain tumors and other pathologies [8–12]. DSC-MRI has been shown to predict tumor grade [13–15] and predict survival in low-grade gliomas [16], but preliminary evaluations in anti-angiogenic therapies have not been particularly fruitful. CBV, CBF, and MTT are typically quantified using a standard singular value decomposition (sSVD) technique for deconvolving the measured DSC signal from an arterial input function (AIF). However, this sSVD technique has been shown to be sensitive to contrast agent delay and dispersion, leading to errors in DSC-derived parameters. Specifically, the tracer may arrive earlier or later in some tissues than in the AIF, which can lead to an over- or underestimation of CBF in some cases, respectively [17]. To account for this, some studies have utilized a block-circulant matrix for singular value decomposition (cSVD) [18]. This method provides time-invariant perfusion parameter estimates that are independent of the delay between the AIF and the tracer arrival time in tissue. However, both the sSVD and cSVD methods rely on using a single global threshold value for truncating the number of small singular values before decomposition. This problem can be mitigated by using a semi-adaptive oscillation-index cSVD (oSVD) technique, in which the truncation cutoff is minimized on a voxel-wise basis rather than globally [19]. This allows for the most robust and accurate estimation of DSC-derived parameters among SVD techniques. More recently, a Bayesian deconvolution method for estimation of DSC-derived parameters has been described, which is also time-invariant and uses a voxel-wise truncation but has been shown to be more accurate and robust than the oSVD method, at a cost of increased calculation time [20–22]. Although phantom testing and application in some human studies have shown the more advanced Bayesian and oSVD methods provide improved measures of DSC-derived parameters, these deconvolution techniques have not been widely applied to brain tumor perfusion data.

In the current study we examined three perfusion parameters (CBV, CBF, and MTT) in a cohort of recurrent GBM patients using DSC-MRI acquired before and after treatment with bevacizumab. We hypothesized that tumors would demonstrate a marked decrease in CBV and CBF following bevacizumab treatment, and that measures of CBV, CBF, and MTT may provide value for stratifying progression-free (PFS) and overall survival (OS) in recurrent GBM patients. In particular, we hypothesized a larger decrease in CBV and CBF after treatment will be indicative of greater efficacy of the anti-angiogenic therapy, resulting in increased survival. We also hypothesize that the more robust oSVD and Bayesian deconvolution methods will provide more clinically meaningful measures of CBF and MTT compared with the sSVD method, as evaluated by their ability to stratify PFS and/or OS.

Materials and methods

Patients

We examined 45 recurrent GBM (WHO grade IV) patients in this study (Mean age, 57; Age range, 28–75; Mean KPS, 79; 23 at first recurrence, 17 at second recurrence, and 5 at third recurrence). MRI data was acquired within 1 month before and 2 months after treatment with bevacizumab (Mean time before treatment for pre-treatment scan, 6 ± 8 days; mean time after treatment for post-treatment scan, 30 ± 14 days). Patients were treated with intravenous bevacizumab at 10 mg/kg every 14 days. At the time of last evaluation on Sep. 19, 2014, 40 out of 45 patients had progressed and 34 out of 45 patients were deceased. All patients gave informed written consent to have their information contained in our UCLA institutional review board (IRB) approved neuro-oncology database.

MRI

All MRI images were collected on either a 1.5T (Siemens Avanto or Sonata, Erlangen, Germany; GE Medical Systems Excite LX or HDx, Waukesha, WI) or 3T MR scanner (Siemens Trio, Verio, or Skyra, Erlangen, Germany). Standard clinical images were obtained for all patients, including T1-weighted, T2-weighted, and fluid-attenuated inversion recovery (FLAIR) images. A 0.025 mmol/kg preload dose of gadolinium contrast agent was administered prior to DSC-MRI to diminish contrast agent extravasation. A 3–5 cc/sec bolus of either gadopentetate dimeglumine (Gd-DTPA; Magnevist, Bayer Schering Pharma, Leverkusen, Germany), administered at a dose of 10–20 cc (0.075 mmol/kg), or gadobenate dimeglumine (Gd-BOPTA; Multihance, Bracoo Diagnostics, Princeton, NJ), administered at a dose of 9–20 cc (0.075 mmol/kg), was used for DSC acquisition and subsequent T1-weighted post-contrast (T1 + C) images (total of 0.01 mmol/kg) using a power injector. DSC scan parameters varied slightly depending on the particular scanner used. Echo times (TE) ranged from 23–50 ms, repetition times (TR) ranged from 1250–1400 ms, flip angle ranged from 30–35°, data included 40–90 temporal timepoints at a slice thickness of 4–6 mm with an interslice gap of 0–1 mm. A total of 6–25 slices were collected through the tumor at matrix sizes ranging from 80×96 to 128×128.

Image analysis

All perfusion data used in this study had full coverage of the tumor based on abnormal enhancement in the T1 + C image. The tumor region of interest was defined by subtracting the T1-weighted image from the T1 + C image to generate a T1 subtraction map, then using a semi-automated thresholding technique followed by manual adjustment of the contour [23]. DSC data was processed using the perfusion analysis software package in Olea Sphere (Olea Medical, Cambridge, MA). Data first underwent preprocessing consisting of motion correction followed by spatial and temporal filtering. The AIF was generated automatically by the software for each individual using a global clustering method which examines the time series for all voxels and identifies a suitable AIF based on their area under the curve, their roughness, and their first moment, without the use of a model AIF, as described by Mouridsen et al. [24] The four deconvolution techniques (sSVD, cSVD, oSVD, and Bayesian) were then applied to the pre-processed data to generate maps of MTT, relative CBF (RBF), and leakage-corrected relative CBV (RBV) [15]. RBF and RBV are relative because the absolute values of these parameters can only be determined up to a multiplicative constant. (Although the maps generated by Olea Sphere are reported in this study as being in units of ml/100 ml/min and ml/100 ml for RBF and RBV respectively, these measurements should still be thought of as relative rather than absolutely quantitative, since these values have not been calibrated or verified to be accurate.) The MTT, RBF, and RBV maps were manually registered to their corresponding pre- and post-treatment T1 + C images using *tkregister2* (Freesurfer, surfer.nmr.mgh.harvard.edu; Massachusetts General Hospital, Harvard Medical School). Median MTT, RBF, and RBV for each of the four deconvolution techniques were pulled from the defined tumor region on pre-and post-treatment images for all patients. RBV maps were identical among deconvolution techniques in all cases, as the calculated blood volume is only dependent on the area under the R2* curve.

Statistics

For the pre- and post-treatment MTT and RBF data, we first applied a Shapiro–Wilk normality test to determine whether the data were distributed normally. Because approximately half of our calculated variables were not normally distributed, we applied a nonparametric Friedman variance test followed by a Dunn's post hoc test to determine whether the four deconvolution methods produced significantly different measures of MTT or RBF. To determine the similarity between deconvolution methods, the data was also plotted for each deconvolution pairing (i.e. Bayesian vs. oSVD, oSVD vs cSVD, etc.) and regression was performed to determine whether the slope significantly differed from unity.

Univariate analysis was performed on age, KPS, number of prior tumor recurrences (and subsequently the number of failed therapies), and tumor volume using a Cox proportional hazards model to test for differences in PFS and OS. The beginning point of survival was defined as the date the data for a variable was acquired (i.e. pre-treatment date for pre-treatment variables, post-treatment date for post-treatment variables and change in variables). Patients that had not reached the endpoint of PFS or OS were censored during analysis. Each variable (pre-treatment, post-treatment, and change in MTT, RBF, and RBV, for all four deconvolution methods) was then separately used in a Cox proportional hazards model with age, KPS, number of recurrence, and tumor volume as covariates to test for differences in PFS and OS. Variables then also underwent log-rank survival analysis, with the median value of a variable among all patients used as the midpoint for stratification. A multiple comparisons correction was not performed on our P-values as the tested variables are highly interdependent.

Results

Results from the Friedman variance test are shown in Fig. 1. Both pre- and post-treatment MTT and RBF values were significantly different between the four deconvolution methods ($P \backslash 0.0001$). In all cases, this difference was likely due to the large differences between the Bayesian method and the circular deconvolution methods, as well as between sSVD and the circular deconvolution methods. No significant differences were seen between the Bayesian method and sSVD ($P [0.05$), or between cSVD and oSVD ($P [0.05$), for all parameters. The ANOVA post hoc Dunn's test results are also shown in Fig. 1.

Direct comparisons between parameter values in tumors calculated using the four deconvolution methods are shown in Fig. 2. RBF calculated using the Bayesian technique was generally larger than RBF derived using the three SVD methods, with the difference most pronounced at high RBF. Interestingly, pre-treatment MTT was always higher and pre-treatment RBF was always lower when using the cSVD method compared with the sSVD method, and this trend was also true for all but two of the post-treatment MTT and RBF measurements. P-values in Fig. 2 show regression results testing whether there was a 1:1 ratio between methods, with a significant P value ($P \backslash 0.05$) indicating deviation from unity. The slope of the regression line differed greatly from unity for the pre- and post-treatment Bayesian-calculated RBF measurements

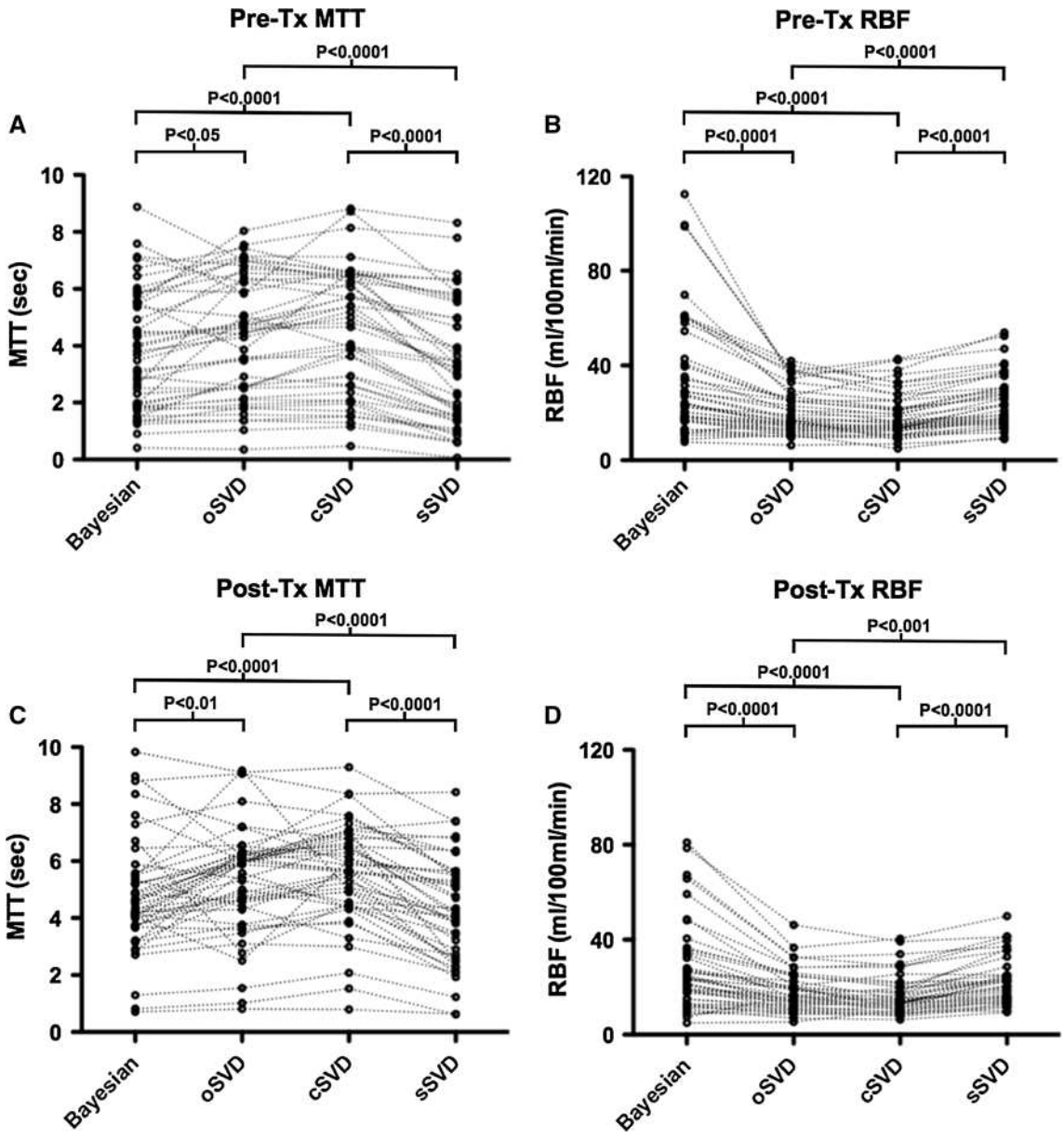

Fig. 1 Comparison of the four deconvolution methods used to calculate pre-treatment MTT (**a**), pre-treatment RBF (**b**), post-treatment MTT (**c**), and post-treatment RBF (**d**). The post hoc Dunn's test results are shown above each plot, with the difference between oSVD and cSVD as well as the difference between Bayesian and sSVD not significant (P[0.05) for all cases

compared with the three SVD-calculated RBF measurements, indicating the largest differences between perfusion parameters estimated using these techniques.

Tumor volume decreased following bevacizumab treatment in 41 out of 47 patients, with a mean reduction of 9.3 ± 16.0 mL. There was no linear correlation between change in tumor volume and time between treatment and post-treatment scan ($P = 0.30$). Age, KPS, and number of recurrence were not significantly correlated with PFS or OS. Pre- and post-treatment tumor volume were highly correlated with PFS ($P = 0.0002$ *and* $P = 0.0003$, *respectively*) but not OS. Change in tumor volume after treatment was not correlated with either PFS or OS.

Tumor RBV decreased following treatment in 26 out of 47 patients. Change in RBV after treatment was able to stratify patients by OS using the proportional hazards model, with a larger decrease in RBV associated with longer survival ($P = 0.0048$). There was no linear correlation between change in RBV and time between treatment and post-treatment scan ($P = 0.59$). Tumor RBF decreased in 25 to 28 out of 45 patients following treatment, depending on the deconvolution method. The proportional

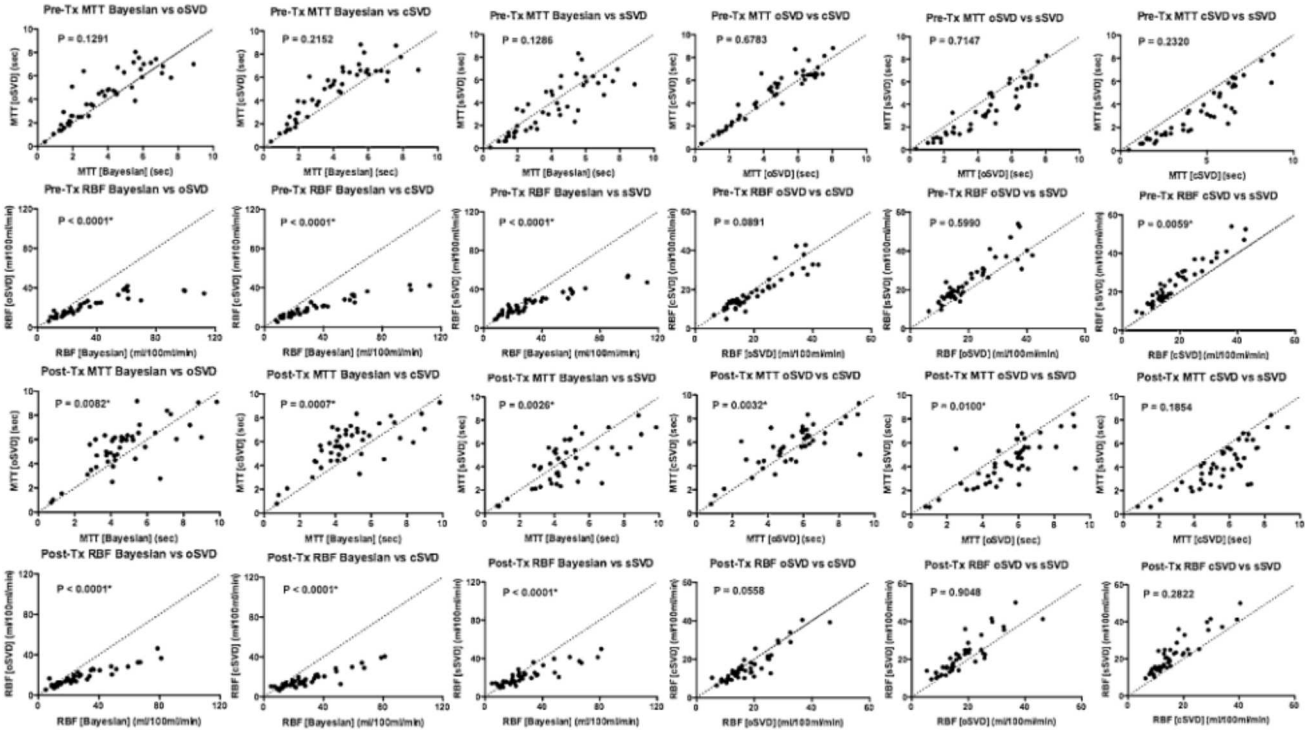

Fig. 2 Linear comparison of different deconvolution methods. *Rows* represent different parameters; *columns* represent pairings of deconvolution methods. P-values shown on each plot are from regression analysis determining whether the slope between variables estimated using different deconvolution methods is significantly different from unity. *Asterisk* denotes P-values below 0.05

hazards model showed pre-treatment RBF was able to significantly stratify patients by PFS using two deconvolution methods (*oSVD*, $P = 0.0315$; *sSVD*, $P = 0.0216$), and significantly stratify patients by OS using all four deconvolution methods (*Bayesian*, $P = 0.0302$; *oSVD*, $P = 0.0120$; *cSVD*, $P = 0.0186$; *sSVD*, $P = 0.0112$), with a higher pre-treatment RBF predictive of longer survival. Additionally, change in RBF following treatment was able to stratify patients by OS for all deconvolution methods, with a greater decrease in RBF predictive of longer survival (*Bayesian*, $P = 0.0207$; *oSVD*, $P = 0.0069$; *cSVD*, $P = 0.0049$; *sSVD*, $P = 0.0079$).

Log-rank analysis of pre-treatment RBF stratified by the median did not show significant stratification of PFS but could stratify OS using all four deconvolution methods, with higher pre-treatment RBF resulting in longer survival (Fig. 3a; *Bayesian*, $P = 0.0052$, *hazard ratio (HR)* $= 2.91$; *oSVD*, $P = 0.0076$, $HR = 2.76$; *cSVD*, $P = 0.0228$, $HR = 2.32$; *sSVD*, $P = 0.0220$, $HR = 2.29$). Change in RBF following treatment was also predictive of OS for all deconvolution methods except sSVD, with a larger decrease in RBF associated with longer survival (Fig. 3b; *Bayesian*, $P = 0.0177$, $HR = 2.34$; *oSVD*, $P = 0.0178$, $HR = 2.34$; *cSVD*, $P = 0.0145$, $HR = 2.39$). Change in RBV following treatment was predictive of both PFS (Fig. 3c, $P = 0.0376$, $HR = 2.00$) and OS (Fig. 3d, $P = 0.0405$, $HR = 2.04$), with a larger decrease in RBV associated with longer survival. P-values from the Cox proportional hazards regression model and the log-rank test are shown in Table 1. An example of a responder (long OS) and a non-responder (short OS) to bevacizumab treatment are shown in Fig. 4.

Discussion

Results from this study suggest that DSC-derived measurements in GBM patients treated with bevacizumab are predictive of survival. Our results demonstrate that change in RBV after therapy is predictive of OS, with a larger decrease in RBV associated with longer survival. This intuitive result supports our original hypothesis, as reductions in tumor-area blood vessel architecture are indicative of the efficacy of the anti-angiogenic bevacizumab therapy. Pre- and post-treatment RBV were not associated with longer survival, which appears different than the results reported by Schmainda et al. [25] where investigators noted that tumors with RBV below a specific threshold, pre- or post-treatment, had improved survival. Interestingly, our results suggest that patients with high cerebral blood flow prior to therapy have a favorable prognosis when treated with bevacizumab. We hypothesize that high pre-treatment RBF

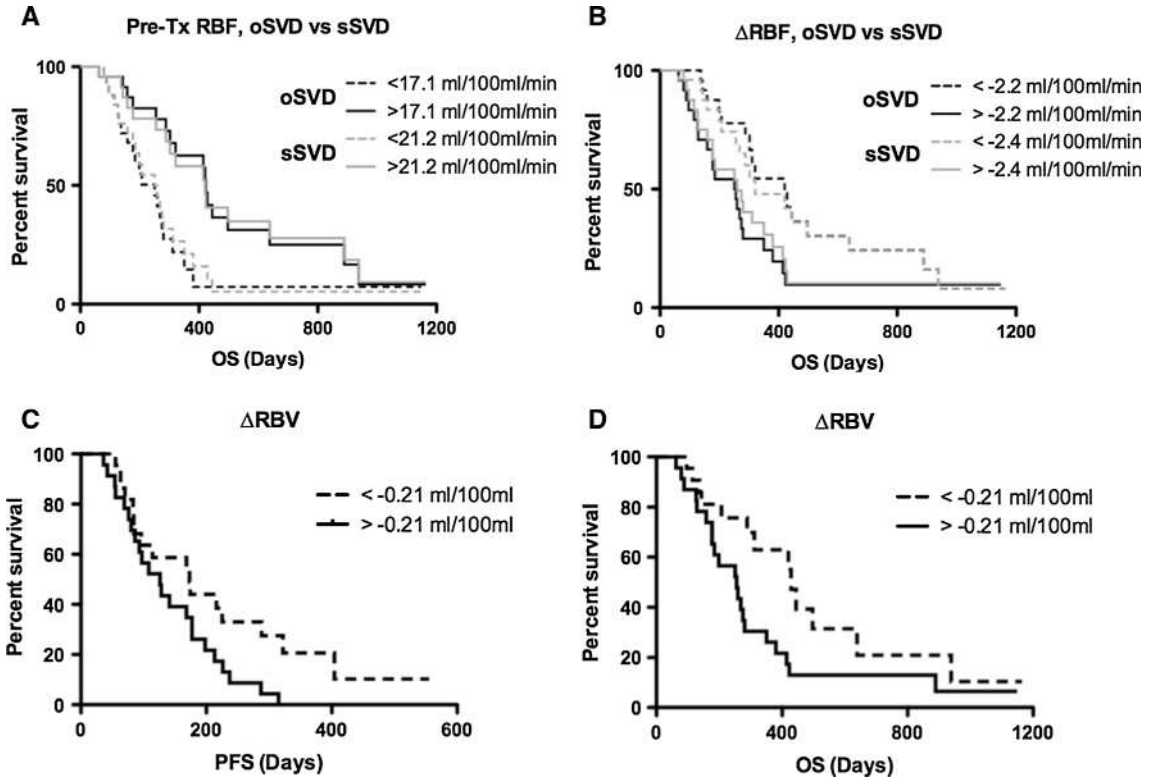

Fig. 3 Pre-treatment RBF (**a**) as well as change in RBF (**b**) stratifies patients by OS, with a circular deconvolution method (oSVD) providing better stratification than the standard deconvolution method (sSVD). Change in RBV between pre- and post-treatment time points stratifies patients by PFS (**c**) and OS (**d**)

Table 1 A Results from the Cox proportional hazards model, B results from log-rank analysis

	Progression-free survival				Overall survival			
	Bayesian	oSVD	cSVD	sSVD	Bayesian	oSVD	cSVD	sSVD
A								
Pre-Tx MTT	0.2984	0.5733	0.6545	0.5141	0.1097	0.7835	0.8875	0.9218
Pre-Tx RBF	0.0767	**0.0315***	0.0577	**0.0216***	**0.0302***	**0.0120***	**0.0186***	**0.0112***
Pre-Tx RBV	0.3322				0.0727			
Post-Tx MTT	0.6627	0.3421	0.4119	0.3643	0.6343	0.7959	0.5983	0.8317
Post-Tx RBF	0.5583	0.4472	0.8253	0.8033	0.8336	0.8164	0.5663	0.7535
Post-Tx RBV	0.9359				0.2264			
DMTT	0.8954	0.3439	0.3943	0.3814	0.6508	0.254	0.7664	0.7859
DRBF	0.1959	0.0734	0.0711	0.0866	**0.0207***	**0.0069***	**0.0049***	**0.0079***
DRBV	0.1896				**0.0048***			
B								
Pre-Tx MTT	0.8219	0.2761	0.1782	0.159	0.8117	0.9313	0.5803	0.8593
Pre-Tx RBF	0.0866	0.1003	0.1817	**0.0482***	**0.0052***	**0.0076***	**0.0228***	**0.0220***
Pre-Tx RBV	0.6891				0.3988			
Post-Tx MTT	0.2366	**0.0117***	0.1037	0.3627	0.4019	0.6125	0.8417	0.5919
Post-Tx RBF	0.4888	0.4581	0.9016	0.6498	0.8803	0.8719	0.5858	0.7809
Post-Tx RBV	0.2035				0.1008			
DMTT	0.3535	0.8167	0.6682	0.7567	0.4017	0.485	0.9324	0.9309
DRBF	0.7647	0.6386	0.3158	0.9596	**0.0177***	**0.0178***	**0.0145***	0.1277
DRBV	**0.0376***				**0.0405***			

* Significance (P\ 0.05)

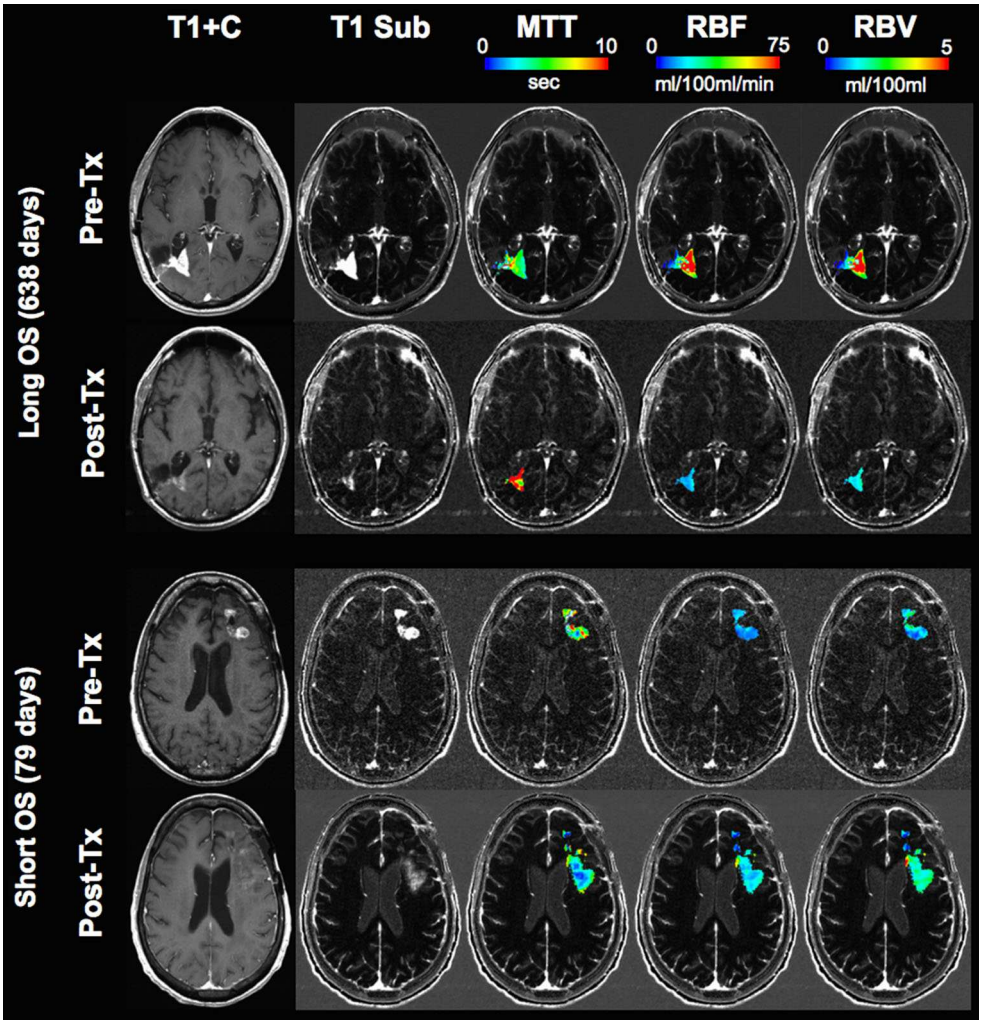

Fig. 4 Example of a responder (long OS) and a non-responder (short OS) to bevacizumab treatment. High pre-treatment RBF and a large decrease in RBF after therapy, as well as a large decrease in RBV after therapy, are associated with longer OS. These maps were calculated using the oSVD method

may improve survival by increasing concurrent chemotherapeutic drug delivery. Additionally, our results demonstrate that a decrease in blood flow after bevacizumab therapy is predictive of longer OS. This effect appears to be driven primarily driven by the pre-treatment RBF measurements, as no association was observed between post-treatment RBF and survival. This may indicate that the blood vessel architecture is typically diminished by therapy in patients with initially high RBF, reducing post-treatment RBF to similar levels in most patients regardless of pre-treatment RBF. Our results appear to be contradictory to a recent study by Batchelor et al. involving newly diagnosed GBM patients treated with cediranib, where they noted longer survival in patients with increased RBF following treatment. This study, however, involved recurrent GBM patients and a different anti-angiogenic agent.

Our results suggest that RBF tends to be overestimated when using sSVD compared to the other time-invariant techniques. Conversely, MTT was typically underestimated using the sSVD technique compared with circular deconvolution techniques. This observation may be due to damaged or abnormal vasculature within the tumor regions, in which the tumor tissue bolus peak may occur earlier than that of the AIF automatically generated by the software. As generation of the AIF is an imperfect process and can vary depending on the software used, mathematical models that remove the timing dependence of the AIF can produce more robust perfusion measurements. The concentration–time curves in perfusion imaging are also influenced by the permeability and tortuosity of the blood vessels; while permeability is modeled and accounted for during data analysis by the leakage correction [15], perfusion processing software does not often account for vessel tortuosity, although models for tortuosity do exist [26].

There were several important limitations to the current study that should be noted. First, the pre-treatment and post-treatment scans were acquired at variable times before and after the start of treatment for each patient, and the post-treatment scan was acquired on average approximately 1 month after treatment. In a more controlled

study, we may have desired to acquire the pre-treatment time point a day prior to treatment and the post-treatment time point within a week following treatment for all patients. Additionally, we did not apply a multiple comparisons correction to the data due to the high correlation of the variables with one another, especially among similar variables calculated using the different deconvolution methods; however, the trends in our data as seen in Table 1 are fairly consistent. Lastly, the DSC scan protocols used in our study varied between patients and scan dates, including a varying number of slices and slice thicknesses. In a more ideal prospective study, these parameters should be standardized to improve consistency in the data. However, as only patients and scan dates with DSC covering the full extent of the tumor for both pre- and post-treatment scans were used in this study, this problem does not seem to have impeded the evidence that our DSC-derived maps can be predictive of outcome.

In conclusion, the deconvolution method used to calculate MTT and RBF had a significant effect on the resulting maps, with RBF overestimated using the sSVD and Bayesian methods compared to the circular deconvolution methods. RBF and RBV calculated from DSC-MRI data were able to stratify GBM patients by PFS and OS following bevacizumab treatment.

Acknowledgments National Brain Tumor Society Research Grant (BME, TFC); NIH/NCI 1 R21 CA167354-01 (BME); UCLA Institute for Molecular Medicine Seed Grant (BME); UCLA Radiology Exploratory Research Grant (BME); University of California Cancer Research Coordinating Committee Grant (BME); ACRIN Young Investigator Initiative Grant (BME); Art of the Brain (TFC); Ziering Family Foundation in memory of Sigi Ziering (TFC); Singleton Family Foundation (TFC); and Clarance Klein Fund for Neuro-Oncology (TFC).

Conflict of interest Drs. Timothy F. Cloughesy, Albert Lai, Whitney Pope, and Benjamin Ellingson are paid consultants for Genentech, Inc., and Hoffman-La Roche, Ltd. Drs. Ellingson and Pope are also a paid consultant for MedQIA, LLC.

References

1. Becker KP, Yu J (2012) Status quo–standard-of-care medical and radiation therapy for glioblastoma. Cancer J 18:12–19
2. Dolecek TA, Propp JM, Stroup NE, Kruchko C (2012) CBTRUS statistical report: primary brain and central nervous system tumors diagnosed in the United States in 2005–2009. Neuro Oncol 14(Suppl 5):v1–49
3. Johnson DR, O'Neill BP (2012) Glioblastoma survival in the United States before and during the temozolomide era. J Neurooncol 107:359–364
4. Stupp R, Mason WP, van den Bent MJ, Weller M, Fisher B, Taphoorn MJ, Belanger K, Brandes AA, Marosi C, Bogdahn U, Curschmann J, Janzer RC, Ludwin SK, Gorlia T, Allgeier A, Lacombe D, Cairncross JG, Eisenhauer E, Mirimanoff RO (2005) European Organisation for R, Treatment of Cancer Brain T, Radiotherapy G, National Cancer Institute of Canada Clinical Trials G: radiotherapy plus concomitant and adjuvant temozolomide for glioblastoma. N Engl J Med 352:987–996
5. Holash J, Maisonpierre PC, Compton D, Boland P, Alexander CR, Zagzag D, Yancopoulos GD, Wiegand SJ (1999) Vessel cooption, regression, and growth in tumors mediated by angiopoietins and VEGF. Science 284:1994–1998
6. Millauer B, Shawver LK, Plate KH, Risau W, Ullrich A (1994) Glioblastoma growth inhibited in vivo by a dominant-negative Flk-1 mutant. Nature 367:576–579
7. Plate KH, Breier G, Risau W (1994) Molecular mechanisms of developmental and tumor angiogenesis. Brain Pathol 4:207–218
8. Young RJ, Gupta A, Shah AD, Graber JJ, Chan TA, Zhang Z, Shi W, Beal K, Omuro AM (2013) MRI perfusion in determining pseudoprogression in patients with glioblastoma. Clin Imaging 37:41–49
9. Server A, Orheim TE, Graff BA, Josefsen R, Kumar T, Nakstad PH (2011) Diagnostic examination performance by using microvascular leakage, cerebral blood volume, and blood flow derived from 3-T dynamic susceptibility-weighted contrast-enhanced perfusion MR imaging in the differentiation of glioblastoma multiforme and brain metastasis. Neuroradiology 53:319–330
10. Ulmer S, Liess C, Kesari S, Otto N, Straube T, Jansen O (2009) Use of dynamic susceptibility-contrast MRI (DSC-MRI) to assess perfusion changes in the ipsilateral brain parenchyma from glioblastoma. J Neurooncol 91:213–220
11. Young R, Babb J, Law M, Pollack E, Johnson G (2007) Comparison of region-of-interest analysis with three different histogram analysis methods in the determination of perfusion metrics in patients with brain gliomas. J Magn Reson Imaging 26:1053–1063
12. Ulmer S, Hartwigsen G, Riedel C, Jansen O, Mehdorn HM, Nabavi A (2010) Intraoperative dynamic susceptibility contrast MRI (iDSC-MRI) is as reliable as preoperatively acquired perfusion mapping. Neuroimage 49:2158–2162
13. Aronen HJ, Gazit IE, Louis DN, Buchbinder BR, Pardo FS, Weisskoff RM, Harsh GR, Cosgrove GR, Halpern EF, Hochberg FH et al (1994) Cerebral blood volume maps of gliomas: comparison with tumor grade and histologic findings. Radiology 191:41–51
14. Maeda M, Itoh S, Kimura H, Iwasaki T, Hayashi N, Yamamoto K, Ishii Y, Kubota T (1993) Tumor vascularity in the brain: evaluation with dynamic susceptibility-contrast MR imaging. Radiology 189:233–238
15. Boxerman JL, Schmainda KM, Weisskoff RM (2006) Relative cerebral blood volume maps corrected for contrast agent extravasation significantly correlate with glioma tumor grade, whereas uncorrected maps do not. AJNR Am J Neuroradiol 27:859–867
16. Law M, Oh S, Babb JS, Wang E, Inglese M, Zagzag D, Knopp EA, Johnson G (2006) Low-grade gliomas: dynamic susceptibility-weighted contrast-enhanced perfusion MR imaging–prediction of patient clinical response. Radiology 238:658–667
17. Calamante F, Gadian DG, Connelly A (2000) Delay and dispersion effects in dynamic susceptibility contrast MRI: simulations using singular value decomposition. Magn Reson Med 44:466–473
18. Wu O, Ostergaard L, Weisskoff RM, Benner T, Rosen BR, Sorensen AG (2003) Tracer arrival timing-insensitive technique for estimating flow in MR perfusion-weighted imaging using singular value decomposition with a block-circulant deconvolution matrix. Magn Reson Med 50:164–174
19. Liu HL, Pu Y, Liu Y, Nickerson L, Andrews T, Fox PT, Gao JH (1999) Cerebral blood flow measurement by dynamic contrast MRI using singular value decomposition with an adaptive threshold. Magn Reson Med 42:167–172

20. Boutelier T, Kudo K, Pautot F, Sasaki M (2012) Bayesian hemodynamic parameter estimation by bolus tracking perfusion weighted imaging. IEEE Trans Med Imaging 31:1381–1395
21. Kudo K, Boutelier T, Pautot F, Honjo K, Hu JQ, Wang HB, Shintaku K, Uwano I, Sasaki M (2014) Bayesian analysis of perfusion-weighted imaging to predict infarct volume: comparison with singular value decomposition. Magn Reson Med Sci 13:45–50
22. Sasaki M, Kudo K, Boutelier T, Pautot F, Christensen S, Uwano I, Goodwin J, Higuchi S, Ito K, Yamashita F (2013) Assessment of the accuracy of a Bayesian estimation algorithm for perfusion CT by using a digital phantom. Neuroradiology 55:1197–1203
23. Ellingson BM, Kim HJ, Woodworth DC, Pope WB, Cloughesy JN, Harris RJ, Lai A, Nghiemphu PL, Cloughesy TF (2013) Recurrent glioblastoma treated with bevacizumab: contrast-enhanced T1-weighted subtraction maps improve tumor delineation and aid prediction of survival in a multicenter clinical trial. Radiology 271:200–210
24. Mouridsen K, Christensen S, Gyldensted L, Ostergaard L (2006) Automatic selection of arterial input function using cluster analysis. Magn Reson Med 55:524–531
25. Schmainda KM, Prah M, Connelly J, Rand SD, Hoffman RG, Mueller W, Malkin MG (2014) Dynamic-susceptibility contrast agent MRI measures of relative cerebral blood volume predict response to bevacizumab in recurrent high-grade glioma. Neuro Oncol 16:880–888
26. Norris DG (2001) The effects of microscopic tissue parameters on the diffusion weighted magnetic resonance imaging experiment. NMR Biomed 14:77–93